International Journal of Fatigue 184 (2024) 108296

Contents lists available at ScienceDirect

International Journal of Fatigue

journal homepage: www.elsevier.com/locate/ijfatigue

A novel fatigue life prediction methodology based on energy dissipation in viscoelastic materials, synergistic effects of stress level, stress ratio, and temperature

A. Vahid Movahedi-Rad *, Lulu Liu, Thomas Keller

Composite Construction Laboratory (CCLab), Ecole Polytechnique Fédérale de Lausanne (EPFL), Station 16, Bâtiment BP, CH-1015, Lausanne, Switzerland

ARTICLE INFO

Keywords:
Fatigue life prediction
Dissipated energy
Cyclic-creep interaction
Temperature effect
Three-dimensional constant life diagrams (3D-CLDs)

ABSTRACT

This work introduces a new methodology to predict the fatigue life of viscoelastic materials by considering the creep effect on fatigue behavior under the concurrent effects of stress level, stress ratio, and temperature. The model established based on the total amount of energy dissipated during fatigue loading. To estimate the amount of dissipated energy under varying stress ratios and temperatures, two shift factors, $\psi_{cyclic}(R,T)$ and $\psi_{creep}(R,T)$, were derived, attributed to the cyclic and creep parts of fatigue loading. These shift factors were subsequently incorporated into defined equilibrium equations to create the relationship between estimated dissipated energy and fatigue life. The input data for the model consisted of the dissipated energy and cyclic creep values obtained from experiments conducted at a reference stress ratio of 0.5 and reference temperature of 20 °C, together with the storage and loss moduli measured from one dynamic mechanical analysis (DMA) experiment in the temperature range of 15 °C–60 °C on a fully-cured epoxy adhesive. To validate the accuracy of the results, the predicted fatigue life at three temperatures of 20 °C, 40 °C and 55 °C, each loaded under three stress ratios of 0.1, 0.5, and 0.9 were compared with the experiments conducted under the same conditions. Almost all predicted results were in good agreement with the experiments, nevertheless; at the stress ratio of 0.9 at 20 °C, due to the significant change in the cyclic creep behavior, the accuracy of the prediction was lower. The developed model was used as a new constant life diagram (CLD) formulation, which afterwards was further developed to plot three-dimensional constant life diagrams (3-D $CLDs$) in which the constant life surfaces were a synergistic function of stress ratio and temperature.

1. Introduction

Viscoelastic materials, such as polymers and polymer-based composites, which possess both viscous and elastic characteristics when undergoing deformation [1], find extensive usages in a diverse range of structural and construction applications, including wind turbine rotor blades, aircraft, automotive industries, bridge decks, as well as in sealing, dampers, and bio-based materials [1–6]. In these materials, the environmental parameters such as humidity, exposure to a salt solution, UV level, and ambient temperature can significantly affect their mechanical properties via provoking various aging mechanisms that degrade their physical, chemical and mechanical properties [7–13]. Among the different environmental parameters, temperature stands out as one of the most influential. In this case, depending on the type of the material used, even a few degrees of the temperature change may considerably alter its mechanical properties, including quasi-static properties, impact resistance, creep and fatigue behavior [1,14–16].

Experimentally, it has been well-shown that in the majority of cases, increasing the temperature resulted in a decrease in the yield stress and ultimate tensile strength [8,17–21]. Accordingly, researchers have suggested different methodologies to predict the tensile and compression mechanical properties of viscoelastic materials, e.g. Eyring's and Ree-Eyring theories to predict the yield stress and the materials' strength by proposing shift factors [15,20,22–27]. Very recently, a new methodology was suggested to predict the tensile properties of viscoelastic materials based on the amount of energy dissipated during tensile loading as a synergistic function of temperature and loading/displacement rate [28]. The temperature effect on creep properties of the polymers and polymers-based materials has also been thoroughly investigated. Creep rupture in these materials is generally a combined phenomenon starting from viscoelastic deformation with the molecular rearrangement and primary and secondary bond rupture, leading to micro-crack formation and damage propagation [1,29]. Similar to quasi-static properties and creep behavior, fatigue life was shortened as the temperature

* Corresponding author.
E-mail address: abdolvahid.movahedirad@epfl.ch (A.V. Movahedi-Rad).

https://doi.org/10.1016/j.ijfatigue.2024.108296
Received 8 February 2024; Received in revised form 18 March 2024; Accepted 20 March 2024
Available online 21 March 2024

Nomenclature

$\alpha, \beta, \eta, \gamma, a, b, g, k, n$	model parameters
$\dot{F}$	loading rate
ϵ	strain
ϵ_m	mean strain
ϵ_w	width of triangle base to model hysteresis loop
$\epsilon_{m,f}$	mean strain at failure
$\psi_{creep}(R)$	stress ratio shift factor related to the creep part of the fatigue loading
$\psi_{creep}(R,T)$	stress ratio-temperature shift factor related to the creep part of the fatigue loading
$\psi_{creep}(T)$	temperature shift factor related to the creep part of the fatigue loading
$\psi_{cyclic}(R)$	stress ratio shift factor related to the cyclic part of the fatigue loading
$\psi_{cyclic}(R,T)$	stress ratio-temperature shift factor related to the cyclic part of the fatigue loading
$\psi_{cyclic}(T)$	temperature shift factor related to the cyclic part of the fatigue loading
ψ_{DMA}	ratio of dissipated energy at temperature T with respect to the reference temperature in a DMA experiment
σ	stress
σ_0	creep stress
σ_a	stress amplitude
σ_{max}	maximum stress
σ_m	mean stress
τ	characteristic time
E	cyclic stiffness
E^*	complex modulus
E_{loss}	loss modulus
$E_{storage}$	storage modulus
E_{vis}	total viscoelastic energy
f	frequency
F_a	cyclic load amplitude
N	fatigue cycle
N_f	number of cycles to failure
R	stress ratio
r^2	coefficient of multiple determinations
R_{gas}	universal gas constant
$S-N_f$	maximum stress versus number of cycles to failure
$S-t_f$	maximum stress versus time to failure
t	time
t_f	time to failure
W	total dissipated energy (TDE)
W_{creep}	TDE attributed to creep loading
W_{cyclic}	TDE attributed to cyclic loading
w_{diss}	dissipated energy per cycle
w_{DMA}	dissipated energy obtained from DMA experiment

increased in different types of the viscoelastic materials from polymers to polymer-based composites materials. It has been shown that an increase in temperature considerably degraded the fatigue resistance of neat polypropylene as well as talc filled and short glass fiber reinforced polypropylene [30]. In another study, it was shown that in short fiber composite, fabricated by 50wt% short glass fiber reinforced and polyamide-6T/6I as matrix, the fatigue life was significantly decreased by increasing temperature from 23 °C up to 80 °C [31]. It was also experimentally revealed in carbon fiber/polyimide composite and basalt fiber/epoxy composite that the elevated temperature significantly altered the fatigue damage evolution and the corresponding stiffness degradation response of the fiber reinforced polymer matrix composites [32,33]. The joint effect of temperature and humidity level within a hygrothermal environment can interact and influence the mechanical properties, durability, and long-term performance of viscoelastic materials, especially composite materials [34,35]. For example, it has been reported that the higher temperature can accelerate the diffusion rates of the water molecules and degradation process of the adhesive as well as debonding of the fiber/resin interface [36].

Viscoelastic materials experience various types of loading patterns throughout their lifespan. It is well-documented that the mechanical response of these materials is dependent on the specific type of loading pattern applied to them [37–41]. The sensitivity of viscoelastic materials to the type of the applied loading pattern is attributed to their possession of two distinct sets of mechanical properties: cyclic-dependent and time-dependent mechanical properties [42,43]. The cyclic-dependent mechanical properties of viscoelastic materials, such as fatigue stiffness and hysteresis loop area, can be measured in the high-frequency fatigue experiments conducted under zero mean stress conditions, where the material's time-dependent deformation has a negligible impact. In contrast, the time-dependent mechanical properties are associated with the material's rheology and are measurable by performing creep, recovery or relaxation experiments [1,7]. Other studies further confirm that cyclic- and time-dependent phenomena can interact during cyclic loading, and the degree of their interactions depends on the materials type, applied loading pattern, and environmental factors such as temperature and humidity level [12,14,44].

To present the fatigue data, $S-N_f$ or $S-t_f$ curves are normally used where the variation of the maximum stress, σ_{max}, mean stress σ_m or stress amplitude, σ_a, is plotted against number of cycles to failure, N_f, or the duration of the fatigue experiment up to the failure, t_f, on a semi-logarithmic scale. Apart from $S-N_f$ or $S-t_f$ curves, fatigue life of a material can also be illustrated using constant life diagrams ($CLDs$), which demonstrate the concurrent effect of σ_m and σ_a on the fatigue life of the examined material at different stress ratios (R), defined as the ratio of σ_{min} over σ_{max} [45]. The $CLDs$ are divided into three sectors; $0 < R < 1$ expresses tension – tension ($T-T$) fatigue, $1 < R < +\infty$ represents compression – compression ($C-C$) fatigue, while $-\infty < R < 0$ denotes mixed tension – compression ($T-C$) fatigue loading that can be tension- or compression-dominated.

In order to obtain a satisfactory assessment of the structural fatigue behavior, the development of fatigue prediction methodologies is necessary since conducting the experiments at all the different combinations of fatigue parameters and surrounding temperatures would be costly, time consuming, and in some cases impossible. The majority of the existing models were formulated by considering only the cyclic-dependent mechanical properties, and the role of the time-dependent mechanical properties on fatigue life was ignored, which led to inaccurate fatigue life predictions as the stress ratio increased towards 1.0 [45]. In addition, to simulate the $CLDs$, several models were developed as a predictive tool; however, they have all been formulated based only on the cyclic-dependent mechanical properties [2,45]. In order to obtain more accurate fatigue life predictions at different loading patterns in viscoelastic materials, both cyclic- and time-dependent mechanical proprieties as well as the effect of temperature on them should be considered [14,44,46]. To address the synergistic effect of loading pattern and temperature on the fatigue life of viscoelastic materials by considering both cyclic- and time-dependent mechanical proprieties, Miyano et al. [14] suggested a fatigue life prediction methodology founded on four assumptions; namely, (*i*) the same failure process for static, creep, and fatigue failure; (*ii*) same time–temperature superposition principle for all strengths; (*iii*) linear cumulative damage law for

monotonic loading; and (*iv*) linear dependence of fatigue strength on stress ratio. To implement this model, a certain amount of input data is required, including tensile experiments at different temperatures and strain rates to plot constant strain rate (CSR) master curves, and two sets of $S-t_f$ curves at room temperature, one at the stress ratio of 1.0, obtained from a pure creep experiment, and another from a set of fatigue experiments at a stress ratio of 0.0, and finally, a set of fatigue experiments at a stress ratio of 0.0 at the temperature of interest.

Statistically speaking, fatigue in structures is recognized as a significant problem, and it is well-accepted as the most common failure mechanism in structural components while pure static failure is rarely observed [2,47,48]. However, according to the literature, the main focus of the existing methodologies has been on the prediction of the temperature effect on quasi-static properties and creep behavior of viscoelastic materials while the development of methodologies to predict the temperature effect on fatigue behavior has not been investigated to the same extent. This might be due to the fact that fatigue behavior in viscoelastic materials is not an easy issue to deal with, especially when the role of the creep is highlighted. As has been discussed in previous works, to improve the accuracy of fatigue life prediction in viscoelastic materials, especially for stress ratios close to 1.0, it is necessary to incorporate time-dependent mechanical properties into fatigue prediction methodologies [14,44,46]. This point was addressed in [46] in which the suggested model simulated the $S-t_f$ curves and CLD by considering both time- and cyclic- dependent mechanical properties. However, incorporating the temperature effect makes the prediction of the fatigue behavior even more complex, since it requires that the effect of the stress level, stress ratio and temperature are jointly observed. To implement the model suggested by Miyano et al. [14], as has been mentioned, a wide range of input data is required. Additionally, this model was founded based on the linear cumulative damage law as well as the linear dependence of fatigue strength on stress ratio, while the behavior of many polymers and polymer-based composites is characterized by a nonlinear viscoelasticity, especially at high stress levels and elevated temperatures [1,43]. Furthermore, these materials do not follow a linear cumulative damage law if cyclically loaded, due to the complexity of the damage process [2,44]. Besides, the nonlinear nature of the interactions between time- and cyclic-dependent mechanical properties leads to a nonlinear relationship between the stress ratio and fatigue behavior [38,44,46].

The objective of this study is to develop a modeling methodology to concurrently predict the fatigue life of viscoelastic materials at an arbitrary combination of stress levels and stress ratios and surrounding temperatures by considering the creep effect on fatigue behavior. Another objective of this study is to minimize the input data required for the model, achieved by utilizing only one $S-t_f$ curve at room temperature, and avoiding the need for high-temperature fatigue experiments. To achieve the mentioned aims, the application of the previously developed model, [46], is extended in this work. The model is applied to an epoxy adhesive. As input data, the experimental results at the stress ratio 0.5 at 20 °C together with a dynamic mechanical analysis (DMA) experiment in the temperature range from 15 °C to 60 °C, to cover both glassy and glassy-to-rubbery transition states, were employed to determine the model parameters and consequently to predict the number of cycles to failure. The accuracy of the predictions was evaluated by comparing the predicted results at stress ratios of 0.1, 0.5 and 0.9 at each of three temperatures; 20 °C, 40 °C and 55 °C, with experimental results obtained for the same conditions. In this work, a novel three-dimensional CLD formulation is also developed by expanding the previously introduced model to better understand the influence of temperature rise on fatigue life as a function of the stress level and stress amplitude. The output of this work may be used for design purposes of viscoelastic materials for the outdoor constructional and structural applications and it provides insights into the fatigue behavior of materials.

2. Fatigue life prediction methodology

The proposed prediction methodology was established based on the amount of the specimen's total dissipated energy (TDE), W, during its life under loading at different stress levels, stress ratios, and temperature. A flowchart illustrating the suggested methodology for predicting fatigue life is shown in Fig. 1. It consists of four steps; starting by importing the input data obtained from fatigue experiments at the reference stress ratio and reference temperature, in which the hysteresis loop areas were recorded and their shifts measured, together with a dynamic mechanical analysis (DMA) measurement where the storage and loss moduli were recorded at the temperature range of interest. Next, the dissipated energy attributed to the cyclic and creep loading from fatigue experiments were calculated along with the complex modulus and dissipated energy from DMA analysis, which led to the estimation of the model's parameters. Following that, the shift factors, $\psi_{cyclic}(R,T)$ and $\psi_{creep}(R,T)$, were derived to predict the dissipated energy at different combinations of the stress level, stress ratio and temperature for cyclic and creep part of fatigue loading, respectively. As output of the model, the $S-t_f$ curves at an arbitrary stress ratio and temperature together with the $CLDs$ were predicted.

2.1. DMA experiment (Temperature effect on viscoelastic behavior)

Dynamic mechanical analysis (DMA) is a testing method used to analyze the mechanical properties of materials, and is particularly valuable for viscoelastic materials, as they respond to dynamic stress or strain. Two main outputs from the DMA experiment are the storage modulus, $E_{Storage}$, and the loss modulus, E_{loss}. $E_{Storage}$ is a measure of the material's ability to store energy and return it when the stress is removed while E_{loss} indicates the amount of the energy dissipated in the material. The complex modulus, which represents a combination of both elastic and viscous responses in viscoelastic materials, obtained from DMA experiment at temperature T, is equal to;

$$E^*(T)=\sqrt{E^2_{Storage}(T)+E^2_{loss}(T)} \tag{1}$$

The ratio of the complex modulus at temperature T, to the complex modulus at the reference temperature T_0, normalized complex modulus, is shown in Eq. (2),

$$\frac{E^*(T)}{E^*(T_0)}=\frac{\sqrt{E^2_{Storage}(T)+E^2_{loss}(T)}}{\sqrt{E^2_{Storage}(T_0)+E^2_{loss}(T_0)}} \tag{2}$$

Eq. (3) shows the amount of the energy dissipated at each cycle, according to [1],

$$w_{DMA}=\pi\sigma_a^2\frac{E_{loss}}{E^{*2}} \tag{3}$$

where σ_a is the stress amplitude in the DMA experiment. The ratio of the amount of the energy dissipated at temperatures T relative to the reference temperature is shown in Eq. (4).

$$\psi_{DMA}=\frac{E_{loss}(T)}{E_{loss}(T_0)}\frac{E^{*^2}(T_0)}{E^{*^2}(T)} \tag{4}$$

Since material deformation is a thermally-activated process, its temperature dependence may follow an Arrhenius type of expression in Eq. (5),

$$\psi_{DMA}=Aexp(-\frac{Q}{R_{gas}T}) \tag{5}$$

where Q is the deformation activation energy, R_{gas} is the universal gas constant, T is temperature in kelvin, and A is the activation parameter. As a result, the value for Q value is obtained according to Eq. (6).

$$Q=-R_{gas}\frac{\partial ln(\psi_{DMA})}{\partial(1/T)} \tag{6}$$

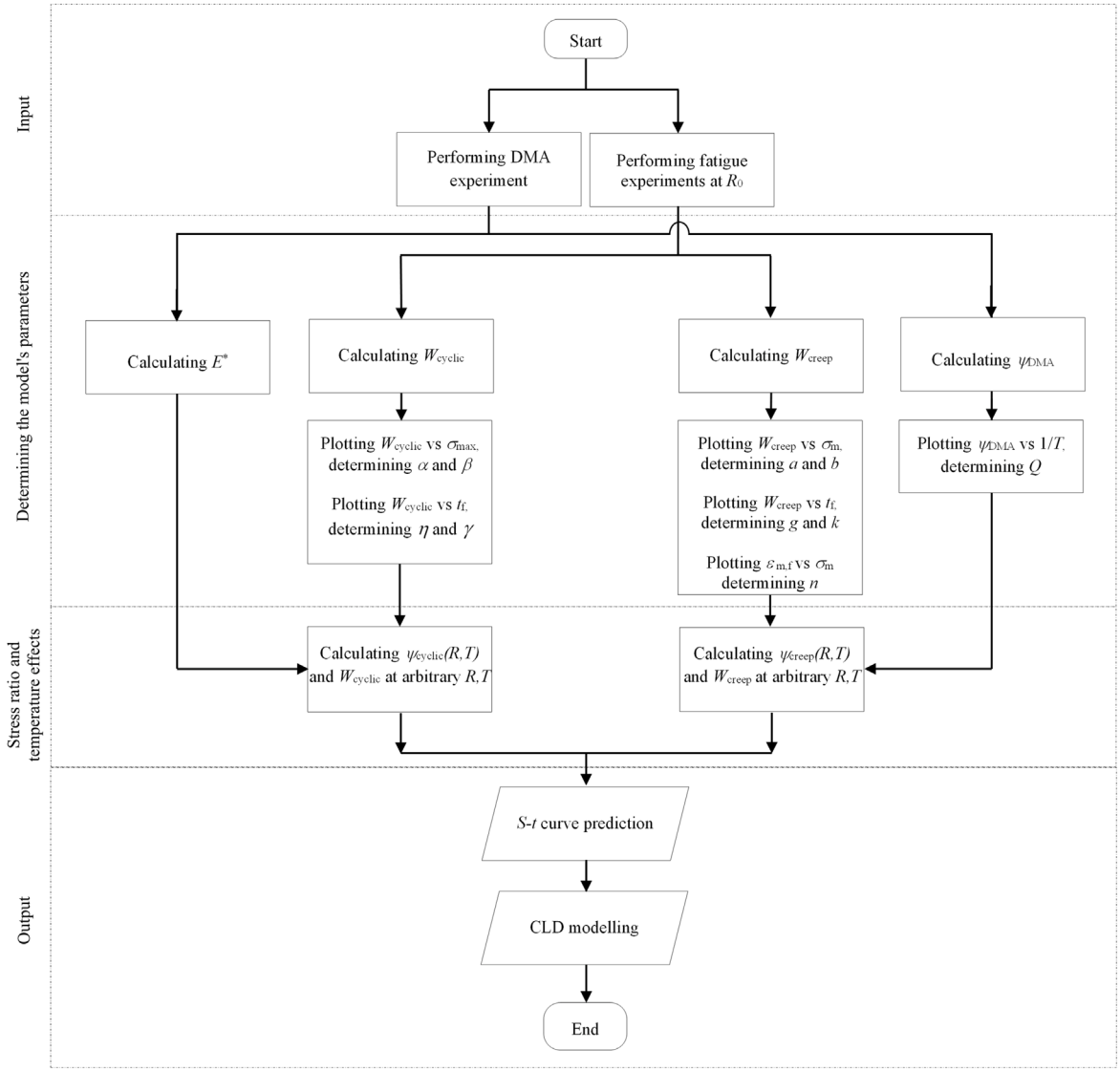

Fig. 1. Flowchart of fatigue life prediction methodology.

2.2. Fatigue experiment

2.2.1. Total dissipated energy (TDE)

In viscoelastic materials, hysteresis loops are formed by applying cyclic loading in the strain–stress coordinate system, as is shown schematically in Fig. 2, in which the slope of each stress–strain hysteresis loop corresponds to the cyclic stiffness, E, and the hysteresis loop shift is considered as an indication of the creep during the cyclic loading, called cyclic creep [12,38,49,50]. The cyclic creep is described by plotting the evolution of the average strain per cycle, ϵ_m, as a function of time, which would be the number of cycles divided by frequency. In the majority of the viscoelastic materials cyclically loaded by an external source in the glassy state, most of the input mechanical energy is recovered when the load is released, which is attributed to the elastic component of deformation [46,51]. A part of the input mechanical energy is, however, dissipated and irrecoverable due to the inelastic component of the deformation, which changes the internal energy of the system as a result of the specimen's structural changes, e.g. the damaging process and/or viscoelastic/plastic deformation, and dissipates the self-generated thermal energy due to the internal friction process [7]. Internal friction is a process in which heat is generated as a result of the resisting frictional forces between the two sides of cracks in a solid material while it undergoes deformation [7,52]. The amount of the dissipated energy per cycle is obtained by measuring the hysteresis area of each cycle [7]. Depending on the material type and loading conditions, the generated heat can facilitate the damage growth and accelerate the viscoelastic deformation by softening the polymeric matrix, which again can lead to damage growth and thermal energy dissipation. Therefore, there is an interrelationship, or thermomechanical coupling, between the extent of the structural changes and amount of thermal energy dissipation [53,54].

In fatigue experiments at the stress ratio of −1.0, energy dissipation was attributed to the cyclic loading alone and therefore W was set equal to W_{cyclic}. At the stress ratio of 1.0, the origin of the energy dissipation was attributed to pure creep and W was set equal to W_{creep}. At other stress ratios, W was set equal to the algebraic sum of W_{cyclic} and W_{creep}, as follows:

$$W = W_{cyclic} + W_{creep} \tag{7}$$

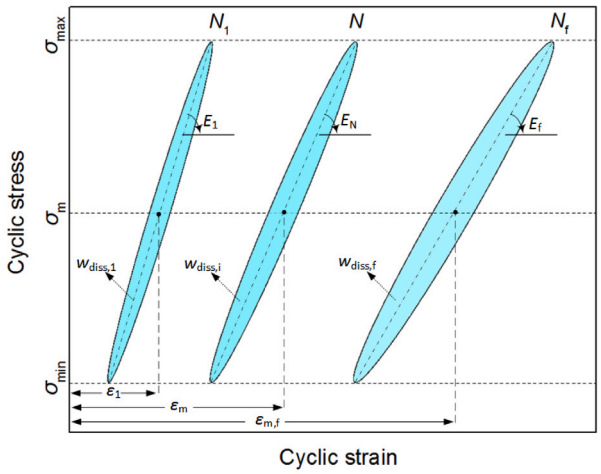

Fig. 2. Schematic representation of hysteresis loops during tension–tension fatigue experiment [46].

W_{cyclic} was defined by the summation of all the individual stress–strain hysteresis areas measured throughout the lifetime of the specimen [7, 55]. Since during a fatigue experiment, all the fatigue cycles cannot normally be recorded, the calculation of W_{cyclic} according to Eq. (8)a is not possible in most cases. Alternatively, W_{cyclic} was obtained here by calculating the area under the graph of w_{diss} versus N from the first to the last cycle according to Eq. (8)b.

$$W_{cyclic} = \sum_{n=1}^{N_f} w_{diss,i} \tag{8a}$$

$$W_{cyclic} = \int_1^{N_f} w_{diss}(N)\, dN \tag{8b}$$

where $w_{diss,i}$ denotes the hysteresis loop area at ith cycle and N_f is the number of cycles to failure. The total creep energy in a viscoelastic material, E_{vis}, is described with the following equation, according to [1]:

$$E_{vis} = \int_0^t \sigma(\tau)\frac{\partial \epsilon(\tau)}{\partial \tau}\, d\tau \tag{9}$$

where τ is the characteristic time. By solving this equation for a specimen loaded under σ_0 with a creep strain of ϵ_f at the moment of failure, W_{creep} is calculated by multiplying σ_0 by ϵ_f, as is shown in Eq. (10).

$$W_{creep} = \sigma_0 \epsilon_f \tag{10}$$

2.2.2. Stress level effect on TDE

Due to the inherent power-law nature of fatigue-related phenomena in relationship to fatigue life [46], the evolution of W_{cyclic} as a function of σ_{max} can be described by Eq. (11)a, in which α and β are the model parameters. In addition, another power-law equation was employed to show the variation of W_{cyclic} with respect to the fatigue life, as it is shown in Eq. (11)b, where η and γ are model parameters, and $t_{f,cyclic} = N_f/f$ where f denotes the fatigue experiment frequency.

$$W_{cyclic} = \alpha \sigma_{max}^{\beta} \tag{11a}$$

$$W_{cyclic} = \eta t_{f,cyclic}^{\gamma} \tag{11b}$$

By setting Eq. (11)a equal to Eq. (11)b, as shown in Eq. (12), the equilibrium equation related to the cyclic part of the fatigue loading is obtained.

$$\alpha \sigma_{max}^{\beta} = \eta t_{f,cyclic}^{\gamma} \tag{12}$$

The variation of w_{creep} versus the fatigue mean stress, σ_m, and creep life were expressed by two separate power-law equations as shown in Eq. (13)a and Eq. (13)b, respectively, in which a, b, g, and k were model parameters.

$$W_{creep} = a\sigma_m^b \tag{13a}$$

$$W_{creep} = g t_{f,creep}^k \tag{13b}$$

The equilibrium equation of the cyclic creep part of the fatigue loading is derived by setting Eq. (13)a and Eq. (13)b equal to each other, as it is shown in Eq. (14).

$$a\sigma_m^b = g t_{f,creep}^k \tag{14}$$

2.2.3. Stress ratio and temperature effects on TDE

Cyclic loading

At constant σ_{max}, as the stress ratio increases, the hysteresis loop area becomes smaller due to the lower stress amplitude, which causes less internal friction. Accordingly, it was assumed that the hysteresis loop area is inversely proportional to the number of cycles to failure [46]. To simulate the effect of the stress ratio and temperature on W_{cyclic}, the stress ratio-temperature shift factor related to the cyclic part of the fatigue loading, $\psi_{cyclic}(R,T)$, is introduced as the amount of dissipated energy per cycle at the stress ratio of R and temperature T, over the amount of dissipated energy per cycle at the reference stress ratio, R_0, and reference temperature, T_0, as shown in Eq. (15).

$$\psi_{cyclic}(R,T) = \frac{w_{diss,i}(R,T)}{w_{diss,i}(R_0,T_0)} \tag{15}$$

To measure the hysteresis loop area, Hahn and Kim [56] suggested an approximation in which each loop is modeled by using two triangles. Fig. 3 shows hysteresis loops at constant σ_{max} for two stress amplitudes and two temperatures schematically. It is seen that this approximation disregarded small parts of each hysteresis loop area. Mathematically, the area of one hysteresis loop, which is equal to two triangles, is shown in Eq. (16).

$$w_{diss}(R,T) = \epsilon_w(R,T)\sigma_a(R) \tag{16}$$

where ϵ_w is the width of the triangle and σ_a is the amplitude of the fatigue cycle. By implementing Eq. (16) into Eq. (15), the following equation is obtained.

$$\psi_{cyclic}(R,T) = \frac{\epsilon_w(R,T)}{\epsilon_w(R_0,T_0)}\frac{\sigma_a(R)}{\sigma_a(R_0)} \tag{17}$$

At constant stress ratio of R, by assuming that the temperature change from T_0 to T would alter the fatigue stiffness from $E(R,T_0)$ to $E(R,T)$, and knowing that, $E \propto (\sigma_a/\epsilon_w)$, the following equation is obtained;

$$\frac{E(R,T)}{E(R,T_0)} = \frac{\sigma_a(R,T)}{\sigma_a(R,T_0)}\frac{\epsilon_w(R,T_0)}{\epsilon_w(R,T)} = \frac{\epsilon_w(R,T_0)}{\epsilon_w(R,T)} \tag{18}$$

Rearranging Eq. (18) leads to the following equation;

$$\epsilon_w(R,T) = \frac{E(R,T_0)}{E(R,T)}\epsilon_w(R,T_0) \tag{19}$$

ψ_{cyclic} is then obtained, by substituting Eq. (19) into Eq. (17), as shown in Eq. (20);

$$\psi_{cyclic}(R,T) = \frac{E(R,T_0)}{E(R,T)}\frac{\epsilon_w(R,T_0)}{\epsilon_w(R_0,T_0)}\frac{\sigma_a(R)}{\sigma_a(R_0)} \tag{20}$$

As it was suggested in [46], at constant temperature, by assuming that the cyclic stiffness is comparable at different stress ratios, $\epsilon_w(R,T_0)$ / $\epsilon_w(R_0,T_0)$ is equal to $\sigma_a(R)$ / $\sigma_a(R_0)$ using Thales's theorem, and Eq. (21) is obtained after using the expression $\sigma_a = \sigma_{max}(1-R)/2$.

$$\psi_{cyclic}(R,T) = \frac{E(T_0)}{E(T)}\left(\frac{1-R}{1-R_0}\right)^2 \tag{21}$$

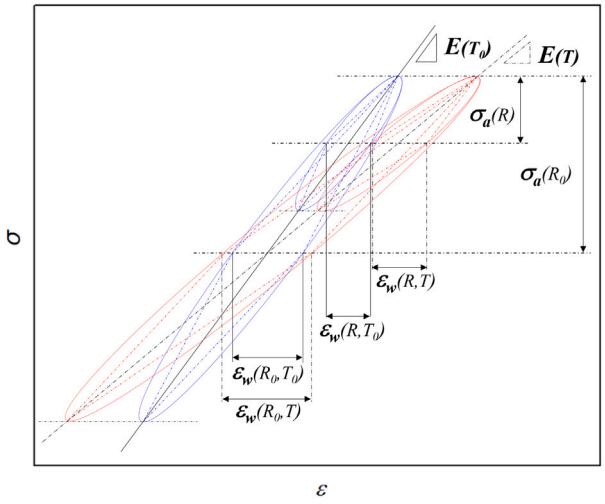

Fig. 3. Schematic representation of fatigue hysteresis loops, loaded under two stress amplitudes of $\sigma_a(R_0)$ and $\sigma_a(R)$, each at two temperatures of T_0 and T, and corresponding approximation of hysteresis loop area by two triangles.

Accordingly, Eq. (21) can be rewritten in to the following form;

$$\psi_{cyclic}(R,T) = \frac{\psi_{cyclic}(R)}{\psi_{cyclic}(T)} \tag{22}$$

in which;

$$\psi_{cyclic}(R) = \left(\frac{1-R}{1-R_0}\right)^2 \tag{23a}$$

$$\psi_{cyclic}(T) = \frac{E(T)}{E(T_0)} \tag{23b}$$

To determine $\psi_{cyclic}(T)$, it is assumed that the variation of fatigue stiffness as temperature changes can be estimated by the variation of the complex modulus obtained from the DMA experiment, which is shown in Eq. (2). By multiplying the derived cyclic shift factor to the right side of Eq. (12), the equilibrium equation related to the cyclic part of the fatigue loading becomes stress ratio and temperature dependent, as shown in Eq. (24);

$$\alpha\sigma_{max}^{\beta} = \psi_{cyclic}(R,T)\eta t_{f,cyclic}^{\gamma} \tag{24}$$

Creep loading

The creep shift factor, $\psi_{creep}(R,T)$, is introduced as the amount of W_{creep} at stress ratio R and temperature T over the reference conditions, according to Eq. (25).

$$\psi_{creep}(R,T) = \frac{W_{creep}(R,T)}{W_{creep}(R_0,T_0)} \tag{25}$$

It is assumed that the variation of the dissipated energy is temperature dependent and it may follow an Arrhenius type of expression.

$$W_{creep}(R,T) = W_0(R)exp(-\frac{Q}{R_{gas}T}) \tag{26}$$

where W_0 is obtained according to Eq. (10). By combining Eq. (10) and Eq. (26) followed by inserting the resulted equation into Eq. (25), Eq. (27) is derived.

$$\psi_{creep}(R,T) = \frac{\sigma_m(R)\epsilon_{m,f}(R)}{\sigma_m(R_0)\epsilon_{m,f}(R_0)}\exp\left(\frac{Q}{R_{gas}}\left(\frac{1}{T_0}-\frac{1}{T}\right)\right) \tag{27}$$

The viscoelastic materials cyclically creep under σ_m, and a power-law function, e.g. Eq. (28), is used to express the stress and creep strain relationship [38,57].

$$\epsilon_{m,f} \propto \sigma_m^n \tag{28}$$

in which n is called the stress exponent. By knowing that $\sigma_m = \sigma_{max}(1+R)/2$ and by introducing Eq. (28) into Eq. (27), $\psi_{creep}(R,T)$ is obtained at constant σ_{max} according to Eq. (29).

$$\psi_{creep}(R,T) = \exp\left(\frac{Q}{R_{gas}}\left(\frac{1}{T_0}-\frac{1}{T}\right)\right)\left(\frac{1+R}{1+R_0}\right)^{1+n} \tag{29}$$

The previous equation can be rewritten in the following form;

$$\psi_{creep}(R,T) = \frac{\psi_{creep}(R)}{\psi_{creep}(T)} \tag{30}$$

in which;

$$\psi_{creep}(R) = \left(\frac{1+R}{1+R_0}\right)^{(1+n)} \tag{31a}$$

$$\psi_{creep}(T) = \exp\left(-\frac{Q}{R_{gas}}\left(\frac{1}{T_0}-\frac{1}{T}\right)\right) \tag{31b}$$

This model suggests that the deformation activation energy needed to calculate $\psi_{creep}(T)$ can be assessed by the amount of the deformation energy obtained from the DMA experiment, as was shown in Eq. (6). The equilibrium equation of the creep part of the fatigue loading is derived by multiplying the right side of Eq. (14), according to Eq. (32);

$$a\sigma_m^b = \psi_{creep}(R,T)gt_{f,creep}^k \tag{32}$$

2.3. Prediction of fatigue life at arbitrary stress ratios and temperature

By rearranging Eq. (24), $t_{f,cyclic}$ is calculated according to Eq. (33).

$$t_{f,cyclic} = \left(\frac{\alpha}{\eta\psi_{cyclic}(R,T)}\right)^{\frac{1}{\gamma}}\sigma_{max}^{\frac{\beta}{\gamma}} \tag{33}$$

In addition, $t_{f,creep}$ is given by Eq. (34), which is obtained by reorganizing Eq. (32);

$$t_{f,creep} = \left(\frac{a}{g\psi_{creep}(R,T)}\right)^{\frac{1}{k}}\sigma_m^{\frac{b}{k}} \tag{34}$$

To predict the $S-t_f$ curve at an arbitrary stress ratio and temperature, Eq. (35) is proposed, in which both $ln(t_{cyclic})$ and $ln(t_{f,creep})$ are taken into account via a linear interpolation:

$$ln(t_f) = \left(\frac{1-R}{2}\right)ln(t_{f,cyclic}) + \left(\frac{1+R}{2}\right)ln(t_{f,creep}) \tag{35}$$

where the loading rate or frequency is constant and $0 < R < 1$. This equation was also used to plot $CLDs$ (see Section 6) in which the predicted $S-t_f$ curves at different stress ratios are employed to simulate the σ_m and σ_a at a specific constant life line of t_f.

3. Experimental data

The application and prediction accuracy of the proposed model were evaluated under tension–tension fatigue loading for an epoxy-based resin with the commercial name SikaDur 330, a commonly used material in structural engineering applications, supplied by SIKA Schweiz AG. The adhesive was produced with a 4:1 resin-to-hardener mixing ratio, as suggested by the manufacturer. Subsequently, the adhesive was poured into aluminum molds of the specimen dimensions. Curing occurred for 24 h under laboratory conditions (T = 25 ± 5 °C, RH = 50 ± 10%), followed by four hours post-curing at 60 ± 0.5 °C in an oven.

To conduct the fatigue experiments on the adhesives, dog-bone specimens according to ASTM D638-14 [58], with gauge length dimensions of 57.0 × 13.0 × 4.0 mm^3 (length × width × thickness) were used in which the grip-to-grip distance was 115 mm. The details of the specimen dimensions are illustrated in Fig. 4.

The fatigue behavior of the adhesive at three stress ratios of 0.1, 0.5, and 0.9, each at three temperatures of 20 °C, 40 °C, and 55 °C were examined. To control the temperature of the environment, all fatigue

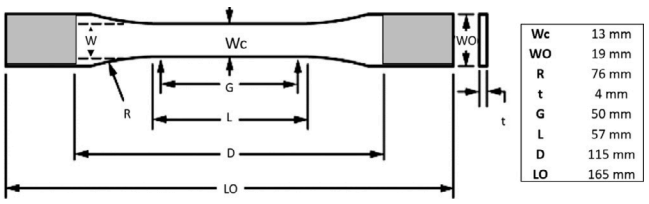

Fig. 4. Specimen dimensions of the epoxy adhesive for fatigue experiment.

experiments were conducted in a chamber, and a fan was employed to circulate the air within the chamber. At each temperature and stress ratio, a wide range of cyclic loads was applied to the specimens in order to cover a wide range of fatigue lives. In addition, at each condition, three specimens were examined. In all fatigue experiments, at the different stress levels, the loading rate, $\dot{F}$, was kept constant at 2.5 kN/s, and accordingly, different frequencies were selected. The frequency, f, of each load level with cyclic load amplitude, F_a, was calculated by solving the following equation:

$$\dot{F} = 4F_a f \tag{36}$$

The variation of the longitudinal strains was measured by a digital image correlation (DIC) (camera Point Grey - Grasshopper3 with a resolution of 2.2 Mpixels and Fujinon HF35SA-1 35 mm F/1.4 lens) with an acquisition frequency of 160 images/s. The video-extensometer measured the relative position of two lines marked on the specimens' surface and calculated the corresponding strain values. For selected cases, the surface temperature of the specimens during the deformation was measured, and no significant self-generated temperature was monitored during the fatigue loading. The data obtained from the fatigue experiments loaded under the stress ratio of 0.5 and at 20 °C was used as input data and all other experiments served to validate the prediction results.

Fig. 5a shows the fatigue hysteresis loops of the studied material loaded at the reference stress ratio of 0.5, under a selected stress level of σ_{max} equal to 24 MPa at 20 °C. As the number of cycles increased, the specimen cyclically crept, which resulted from the viscoelastic deformation of the polymeric matrix as well as the permanent deformation that might have been induced by fatigue damage. The variation of mean cyclic strain versus number of cycles is shown in Fig. 5b, which shows a rapid increase at the early stage of loading, followed by a steady state evolution up to the failure. Fig. 5b also depicts the variation of hysteresis loop area against the number of cycles. It was observed that as the number of cycles increased, hysteresis loop areas were almost constant. According to Eqs. (8) and (10), the values of W_{cyclic} and W_{creep} were calculated as 77.223 and 0.104 MJ/m^3, respectively.

Dynamic mechanical analyses (DMA) were performed to determine the thermomechanical behavior of the studied material. A TA Instruments Q800 dynamic mechanical analyzer in single cantilever configuration was used to perform the experiments. Specimens measuring 35.0 × 10.0 × 3.0 mm^3 (length × width × thickness) were prepared in the same manner as those for the fatigue experiment. Three experiments were carried out on three different specimens in the temperature range of 15 °C to 60 °C with a heating rate of 5 °C/min in an air atmosphere, and the same loading rate at the top and bottom of specimen edges as in the fatigue experiments. Fig. 6 shows the variations of storage and loss moduli versus temperature. It can be seen that the storage modulus gradually decreased as temperature increased; however, the decreasing trend became steeper in the glassy-to-rubbery transition state at temperatures higher than the $T_{g,onset}$, which was around 47 °C. Additionally, the loss modulus did not change significantly at temperatures lower than the $T_{g,onset}$; however, beyond that, it increased considerably.

Table 1
A summary of model parameters for studied epoxy adhesive.

α	β	η	γ	a	b	g	k	n
3.02e+29	−19.69	3.23e−04	1.16	2.54e−03	1.29	0.22	−0.06	0.29

4. Model application

4.1. DMA experiment

The variation of the normalized complex modulus with respect to temperature is depicted in Fig. 7a. In the glassy state, the normalized complex modulus decreased gradually as the temperature increased. A reduction of 15% in the complex modulus was measured as the temperature increased from 20 °C to $T_{g,onset}$. At temperatures greater than the $T_{g,onset}$, the complex modulus decreased more rapidly and at a temperature of about 60 °C, the complex modulus had lost 45% of its 20 °C value.

Fig. 7b shows the evolution of the natural logarithm of ψ_{DMA} plotted against the inverse of the temperature in kelvin. It was observed that the activation energy, which according to Eq. (6) is the slope of the curves multiplied by -R_{gas}, was divided into two regimes: low temperature, attributed to the glassy state of material, and high temperature, related to the transition state. In the low temperature regime, which was in the range from 20 °C up to $T_{g,onset}$, the activation energy was 9.83 kJ/mol while in the high temperature regime, from $T_{g,onset}$ to 60 °C, the activation energy was much higher, at 121.90 kJ/mol.

4.2. Fatigue experiments

The input data for the fatigue experiments, obtained under a stress ratio of 0.5 at 20 °C, was utilized to establish the values of the model parameters, consisting of α, β, γ, a, b, k, g, and n. W_{cyclic} was determined by measuring the area of the hysteresis loops using the formulation presented in Eq. (8). The variation of the obtained W_{cyclic} was plotted against σ_{max} for the studied material in Fig. 8a in a double-logarithmic representation. It was evident that a significant increase in W_{cyclic} occurred as σ_{max} decreased. Through fitting Eq. (11)a to the experimental data points, the model parameters α and β were determined. Eq. (11)b depicts the evolution of W_{cyclic} against t_f in a double-logarithmic coordinate system, in which two other model parameters, η and γ, were estimated by fitting Eq. (11)b to the experimental data points.

By measuring the cyclic creep from the fatigue experiments at the stress ratio of 0.5 at 20 °C, W_{creep} was calculated according to Eq. (10). The evolution of W_{creep} against σ_m is shown in Fig. 9a in a double-logarithmic coordinate system in which a direct relationship between σ_m and W_{creep} was observed. To estimate values for the model parameters a and b, Eq. (13)a was fitted to the experimental data points. In order to determine the model parameters g and k, first the evolution of the W_{creep} against t_f in a double-logarithmic scale was plotted, and then Eq. (13)b was fitted to the experimental data points, as shown in Fig. 9b. The last model parameter, n, was calculated by fitting Eq. (28) to the experimental data points, as is shown by the plot of $\epsilon_{m,f}$ versus σ_m in Fig. 10 on a double-logarithmic scale. A summary of all model parameters obtained in the different materials is presented in Table 1.

5. Model validation

The estimated model parameters, as tabulated in Table 1, were inserted into Eqs. (33) and (34) in which two terms of ψ_{cyclic} and ψ_{creep} were determined according to Eqs. (21) and (29), respectively. The values obtained for $t_{f,cyclic}$ and $t_{f,creep}$ were then substituted into Eq. (35) to predict the fatigue life subjected to the stress ratio R and stress levels σ_{max} at temperature T.

Fig. 11 presents $S - t_f$ curves of the examined material, defined as the variation of σ_{max} versus t_f at various stress ratios (0.1, 0.5,

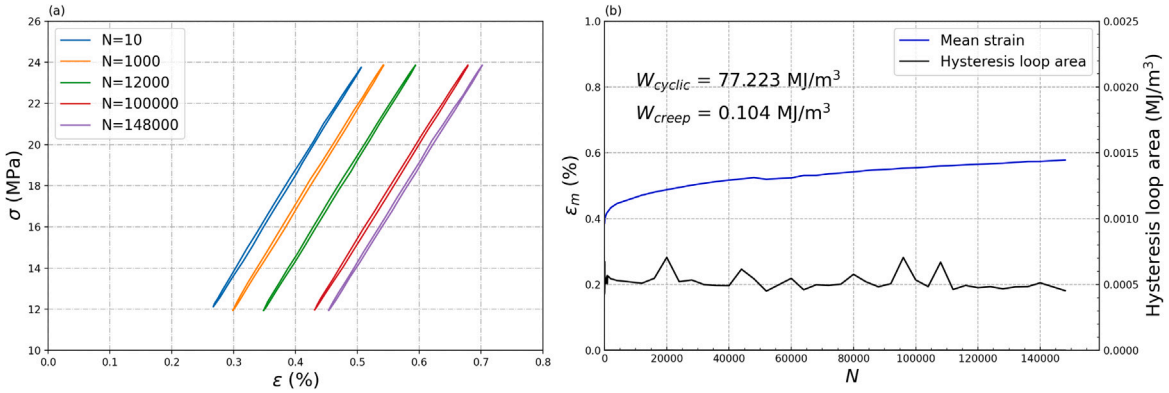

Fig. 5. (a) Fatigue hysteresis loops of epoxy adhesive under a stress ratio of 0.5 and σ_{max} = 24 MPa at 20 °C, and (b) corresponding variations of mean cyclic strain and hysteresis area versus number of cycles.

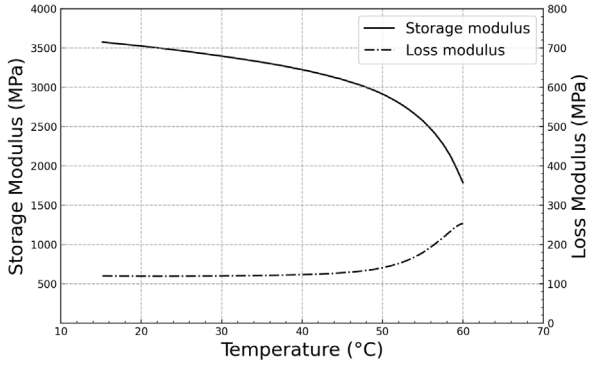

Fig. 6. Variation of storage and loss moduli in the studied epoxy adhesive.

and 0.9) and temperatures (20 °C, 40 °C, and 55 °C). The data points represent the experiments, and the solid curves show the predictions. The predicted $S-t_f$ curves were validated by comparing them with the experimental results. In this case, the accuracy of the predictions at each stress ratio and temperature was quantified by calculating the coefficient of multiple determinations (r^2), where 1.00 represents the highest precision of prediction. The resulting r^2 scores for the different temperatures and stress ratios are displayed in Table 2.

The $S-t_f$ curves at stress ratio 0.1 are shown in Fig. 11a. It can be seen that the predicted fatigue life successfully followed the experimental data points at 20 °C, 40 °C, and 55 °C, as quantitatively indicated by high r^2 scores of 0.866, 0.856, and 0.822, respectively. However, the model slightly overestimated the fatigue life at high-cycle fatigue at 20 °C and 55 °C, and underestimated them at low-cycle fatigue at 40 °C. Fig. 11b shows the $S-t_f$ curves at a stress ratio of 0.5, in which the model was in good agreement with the experiments at 40 °C and 55 °C, resulting in r^2 scores of 0.901 and 0.833. A closer comparison between the experiments and predictions illustrated that the model overestimated the fatigue life at high-cycle fatigue at 55 °C. The accuracy of the model's predictions at a stress ratio of 0.9 was verified by comparing the predicted $S-t_f$ curves at different temperatures with the experimental data points at the same stress ratio, as is shown in Fig. 11c. Experimental observations revealed that slope of the $S-t_f$ curve at 20 °C was much lower in comparison to those observed at 40 °C and 55 °C at this stress ratio, as well as with the $S-t_f$ curves loaded under the stress ratios of 0.1 and 0.5 at different temperatures. Such a considerable change in $S-t_f$ curve, loaded under the stress ratio 0.9 at 20 °C, could be attributed to the pronounced

Table 2
Prediction accuracy at different stress ratios and temperatures in terms of coefficient of multiple determinations (r^2).

	20 °C	40 °C	55 °C
R = 0.1	0.866	0.856	0.822
R = 0.5	1.000*	0.901	0.833
R = 0.9	0.664	0.804	0.813

* Used data.

creep effect on the fatigue behavior due to the high σ_m levels, which was not taken into account by the imported model parameters (Table 1) nor by the ψ_{creep} function. Therefore, the predicted $S-t_f$ curve loaded at the abovementioned conditions was steeper than the trend of the experimental results, which led to an overestimation of fatigue life at low-cycle fatigue and consequently a r^2 score of 0.664. At 40 °C and 55 °C, the predictions followed the experiments well, resulting in r^2 scores of 0.804 and 0.813, respectively; however, they were overestimated at high cycle fatigue values.

6. Model of CLD

The $CLDs$ of the studied material in the tension–tension sector were predicted according to Eq. (35) at three temperatures of 20 °C, 40 °C, and 55 °C and are shown in Fig. 12. The tension–tension sector was bounded by radial lines representing the $S-t_f$ curves at stress ratios between 0.0 and 1.0. $CLDs$ consist of constant life lines, each of which is formed by joining points on consecutive radial lines, all corresponding to a specific fatigue life value [45]. To incorporate the experimental data into the predicted $CLDs$, power curve fitting was performed on all available experimental fatigue data at each stress ratio. In each material, the constant life lines were selected in a range in which the experimental data existed at all three studied stress ratios.

Fig. 12a shows the CLD at 20 °C. It can be seen that at a stress ratio 0.1, there was a good agreement between the simulated constant life lines and the experiments at low and intermediate constant life lines; however, the prediction underestimated the fatigue life at the high constant life line. It was observed that at the stress ratio of 0.9, the experimental data points were close to each other due to the low slope of the $S-t_f$ curve, as shown in Fig. 11c. In this case, the predicted constant life lines underestimated the fatigue life at low constant life line, but were in good agreement at intermediate and high constant life lines.

The predicted CLD at 40 °C is depicted in Fig. 12b where at the stress ratio of 0.1, the predictions were in good agreement with the experiments at the intermediate constant life line, provided overestimated

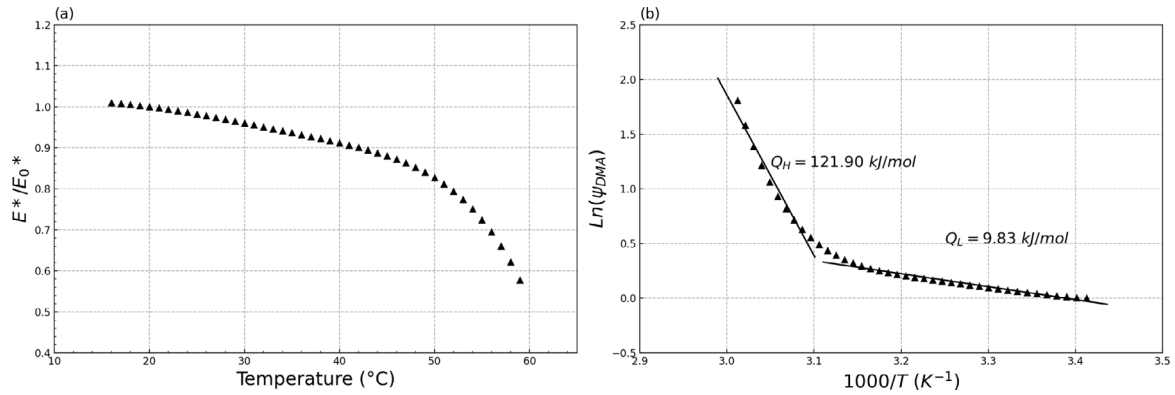

Fig. 7. (a) Variation of normalized complex modulus versus temperature, (b) evolution of natural logarithm of ψ_{DMA} versus inverse of temperature in kelvin.

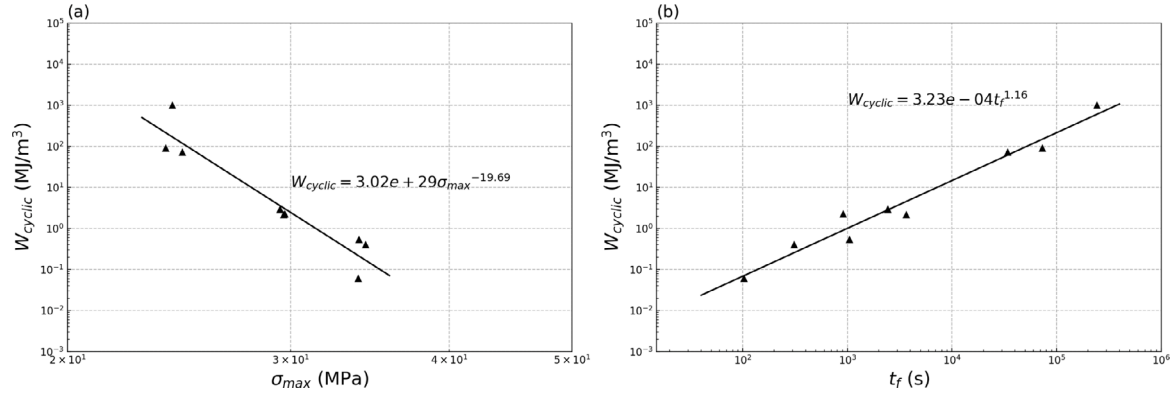

Fig. 8. Evolution of W_{cyclic} versus (a) σ_{max} and (b) t_f loaded under stress ratio 0.5 at 20 °C.

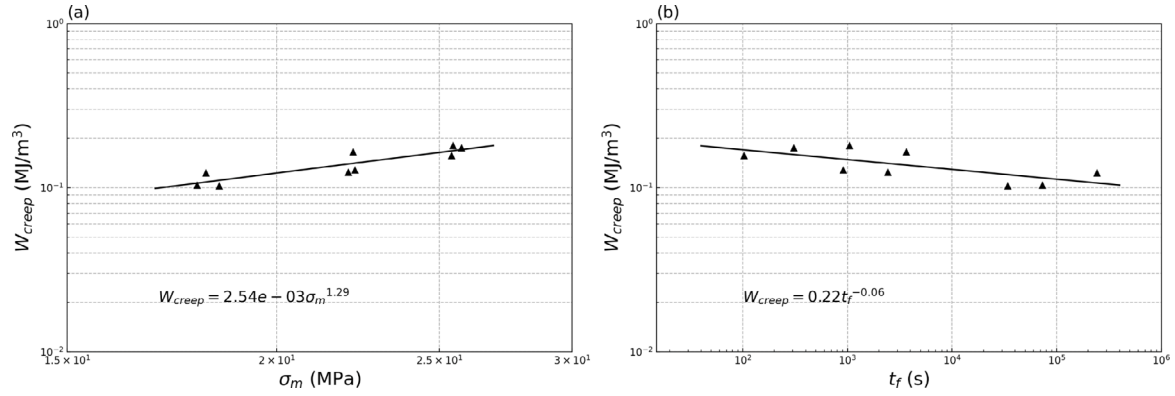

Fig. 9. Evolution of W_{creep} versus (a) σ_m and (b) t_f loaded under stress ratio 0.5 at 20 °C.

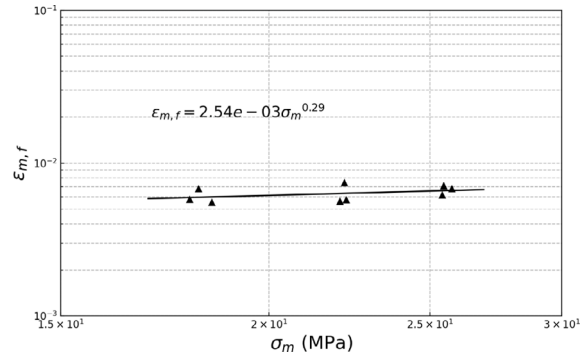

Fig. 10. Evolution of $\epsilon_{m,f}$ versus σ_m loaded under stress ratio 0.5 at 20 °C.

values at the low constant life line, and slightly underestimated values at high constant life line. At a stress ratio of 0.5 the predicted results were accurate at intermediate and high constant lifelines, but provided overestimated values at the low constant life line. At the stress ratio 0.9, at intermediate and high constant life lines, the fatigue life prediction underestimated the fatigue life while at low constant life lines, it closely followed the experiments. The prediction results for temperature 55 °C are illustrated in Fig. 12c. In general, it can be seen that the suggested model at the three studied stress ratios underestimated the fatigue life at high constant lines while it provided good agreement at intermediate and low constant life lines.

Being able to predict the fatigue life at different combinations of stress ratios and temperatures meant that the proposed model was capable of plotting a three-dimensional constant life diagrams (3-D $CLDs$). The 3-D $CLDs$ offers a better assessment of the synergistic

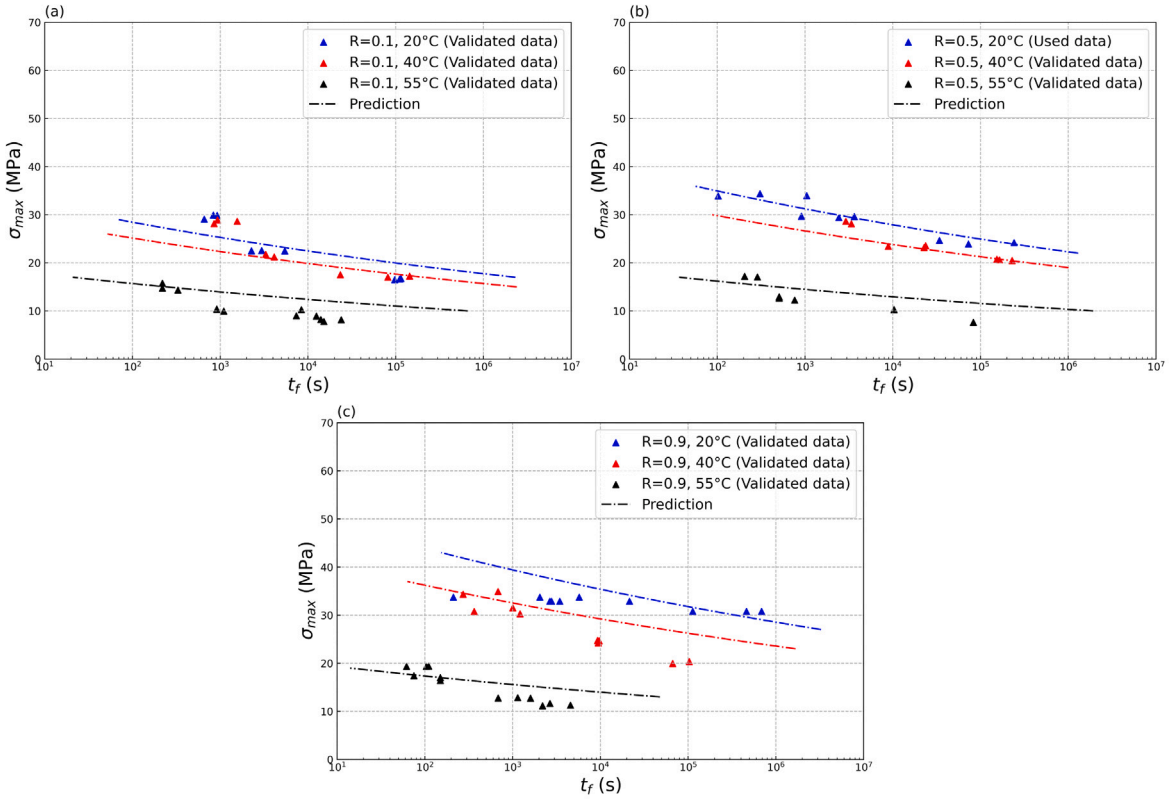

Fig. 11. $S - t_f$ curves showing experimental results and predicted lifetime at different temperatures loaded under stress ratio of (a) 0.1, (b) 0.5, (c) 0.9.

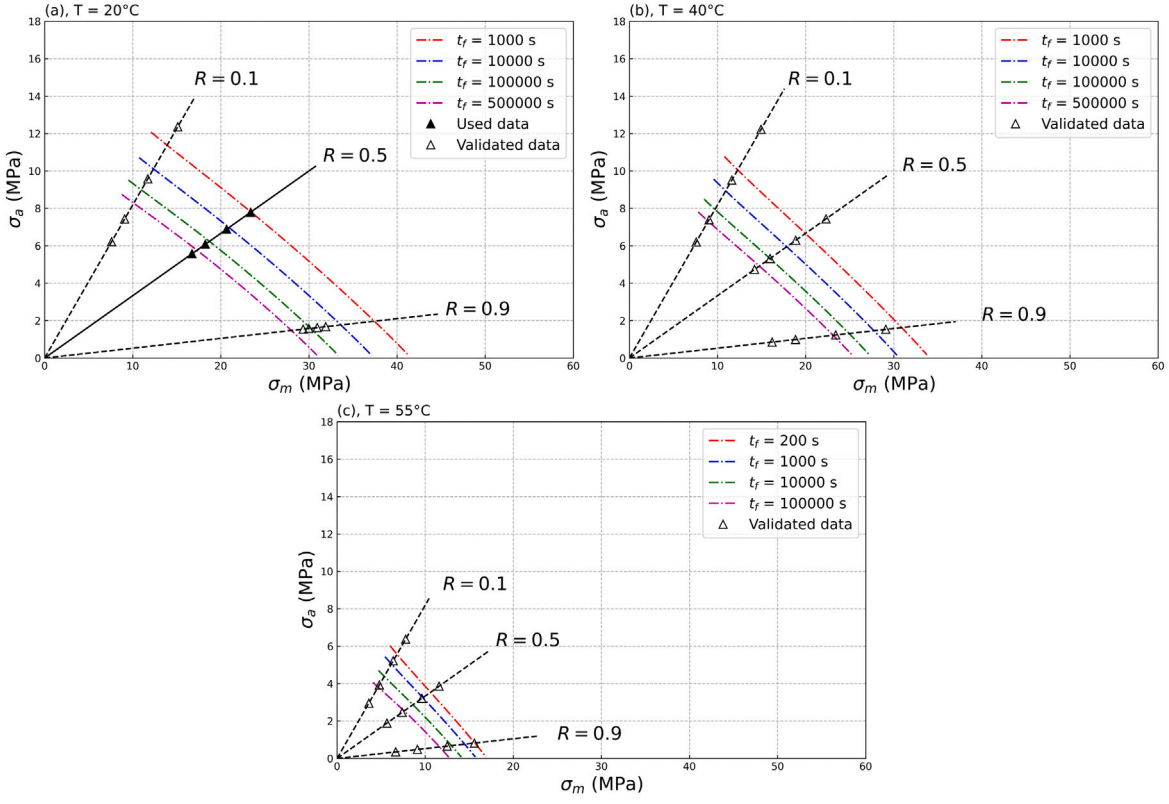

Fig. 12. Constant life diagrams ($CLDs$) at different temperatures (a) 20 °C, (b) 40 °C, and (c) 55 °C.

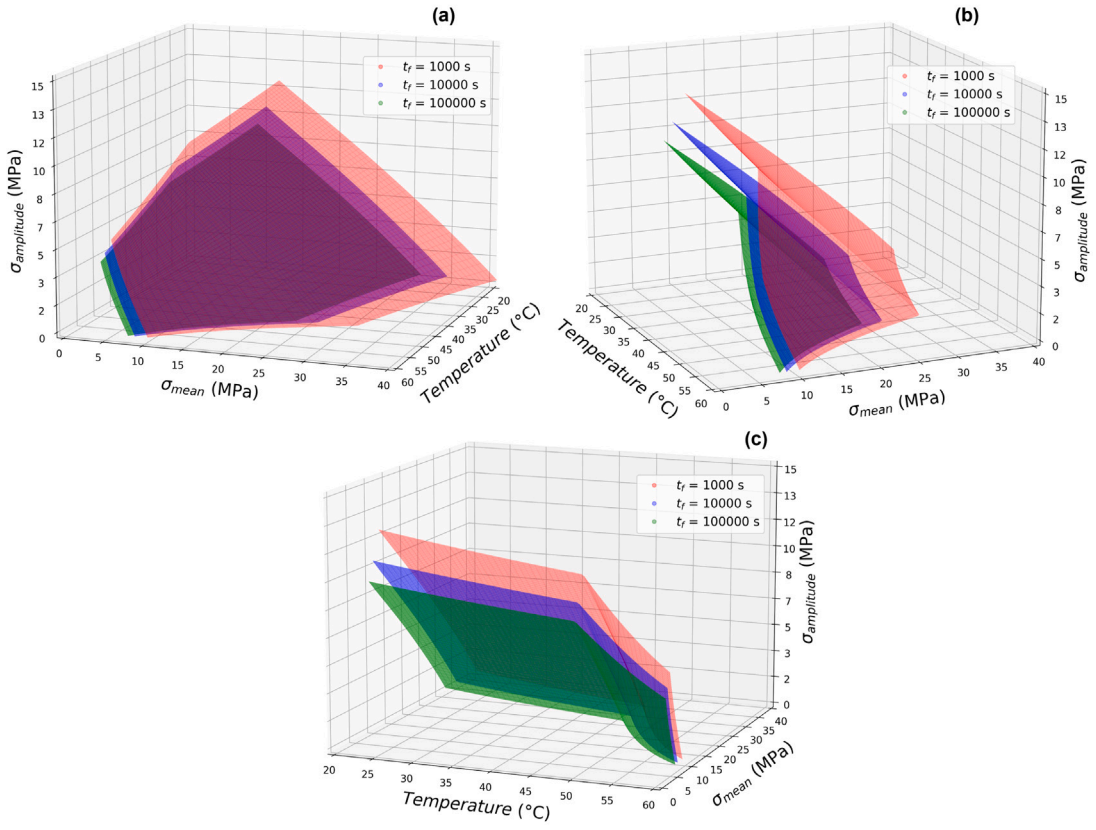

Fig. 13. Three-dimensional Constant life diagrams (3-D CLDs) for constant life surfaces in a range of $t_f = 10^3$ s to 10^5 s at three different perspectives.

effect of temperature and stress ratio on fatigue life of the investigated material in which each surface in a 3-dimensional coordinate system might be called a constant life surface. Fig. 13 shows the 3-D $CLDs$ from different perspectives in the constant life surface range of 10^3 s up to 10^5 s. As the temperature increased, it was noted that the constant life surfaces shifted towards lower values of σ_m and σ_a, indicating a decrease in the fatigue resistance of the material under study. By passing from the glassy state to the transition state, at $T_{g,onset}$, the degradation of the fatigue properties became more pronounced, as was shown by a distinct alteration of the surface gradient of the constant life surfaces, causing the constant life surfaces to approach each another.

7. Model limitations and potential extensions

It has been well-documented that the fatigue behavior of viscoelastic materials in $T-T$ fatigue loading differs from other loading states, e.g. $C-C$ fatigue [45]. Accordingly, the parameters of the model summarized in Table 1 are valid for stress ratios ranging from 0.0 to 1.0, covering $T-T$ fatigue, while these parameters may vary in other loading states. Additionally, the investigated temperature range of the material was in the glassy and glass-to-rubber transition states. At other temperatures, viscoelastic materials may undergo different molecular relaxation processes, such as entering the rubbery state at temperatures higher than T_g [59,60].

While this work focused on predicting the fatigue behavior of one of the most commonly used viscoelastic materials: an epoxy adhesive, the suggested model is also applicable to predict the fatigue behavior of other viscoelastic materials, e.g. rubbers and composites. In the case of composite materials, unlike adhesives, several damage mechanisms, including matrix cracking, matrix/fiber interface debonding, fiber breakage, and delamination, are activated either independently or synergistically during fatigue loading [7,61,62]. In these cases, the contribution of all mentioned damage mechanisms to fatigue life is monitored by the total amount of the dissipated energy. The applicability of the model to predict the fatigue life of glass/epoxy fiber-reinforced polymer composites at room temperature was demonstrated in [46]. Nevertheless, further experimentation and validation would be necessary to confirm the applicability of the model at other temperatures.

In this work, to avoid having the humidity effect on fatigue life, all fatigue experiments were conducted at a constant humidity level, as mentioned in Section 3. However, it is well-documented that changes in humidity levels alter the fatigue behavior of viscoelastic materials [11, 34]. The application of the suggested model can also be extended to consider the effects of humidity levels on fatigue life. This could involve deriving new humidity-shift factors, $\psi(RH)$, to calculate the amounts of dissipated energy at different humidity levels.

8. Conclusions

In this study, a methodology was introduced to predict viscoelastic material fatigue life across various stress levels, ratios, and temperatures, accounting for creep effects. The model predicted fatigue life based on total energy dissipation during fatigue testing, considering cyclic loading (W_{cyclic}) and creep loading (W_{creep}). Energy dissipation was estimated using stress ratio-temperature shift factors ($\psi_{cyclic}(R,T)$ and $\psi_{creep}(R,T)$) incorporated into an equilibrium equation. Experimental data from a single $S-t_f$ curve at a reference stress ratio and temperature, along with storage and loss moduli from a DMA experiment, serve as model inputs. The methodology was applied to

an epoxy adhesive using experimental data at a stress ratio of 0.5 and 20 °C, and DMA results from 15 °C to 60 °C. The model was employed to predict the fatigue life of the epoxy adhesive subjected to the stress ratios of 0.1, 0.5, and 0.9 at temperatures of 20 °C, 40 °C, and 55 °C. Accordingly, the following conclusions were drawn:

1. The predicted $S-t_f$ curves were compared with experiments at different conditions. In general, the predictions were in a good agreement with the experiments, supported by high coefficients of multiple determination. Nevertheless, due to the high σ_m values for the experiments at the stress ratio of 0.9 and 20 °C, the cyclic-creep behavior significantly changed, led to a less accurate predictions.
2. The model developed was used as a new CLD formulation and predicted constant life lines at different conditions. The predictions were in good agreement with experiments, nonetheless, in general, the model underestimated the fatigue life at the high constant life lines. In addition, the model showed a lower prediction accuracy under the stress ratio of 0.9 at 20 °C due to the significant change in the slope of the experimental $S-t_f$ curve.
3. This work introduced the first three-dimensional Constant Life Diagrams (3-D $CLDs$) by plotting conventional $CLDs$ at various temperatures. 3-D $CLDs$ showed that fatigue resistance degraded as the temperature increased as the constant life surfaces shifted towards lower values of σ_m and σ_a, which was intensified at temperatures higher than $T_{g,onset}$.
4. In viscoelastic materials, an increase in the stress ratio tends to amplify the creep effect, which could lead to a significant change in material's fatigue behavior. In such instances, it might be possible that the model parameters, describing the slope of cyclic and creep dissipated energy against stress level or fatigue life on a double logarithmic scale, could be influenced by the stress ratio. To address this, new $\psi(R)$ functions could be derived to simulate the stress ratio effects on these parameters, but this would require additional input data.

CRediT authorship contribution statement

A. Vahid Movahedi-Rad: Writing – original draft, Software, Methodology, Formal analysis, Conceptualization. **Lulu Liu:** Writing – review & editing, Validation, Formal analysis. **Thomas Keller:** Writing – review & editing, Validation, Supervision.

Declaration of competing interest

The authors declare that they have no known competing financial interests or personal relationships that could have appeared to influence the work reported in this paper.

Data availability

Data will be made available on request.

Appendix A. Supplementary data

Supplementary material related to this article can be found online at https://doi.org/10.1016/j.ijfatigue.2024.108296.

References

[1] Guedes RM. Creep and fatigue in polymer matrix composites. Woodhead Publishing; 2019.
[2] Vassilopoulos AP, Keller T. Fatigue of fiber-reinforced composites. Springer Science & Business Media; 2011.
[3] Chen Y, Wu D, Li H, Gao W. Quantifying the fatigue life of wind turbines in cyclone-prone regions. Appl Math Model 2022;110:455–74.
[4] D'Antino T, Pisani MA, Poggi C. Fatigue tensile testing of glass fiber-reinforced polymer reinforcing bars. Constr Build Mater 2022;346:128395.
[5] Ayoub G, Zaïri F, Naït-Abdelaziz M, Gloaguen JM. Modeling the low-cycle fatigue behavior of visco-hyperelastic elastomeric materials using a new network alteration theory: Application to styrene-butadiene rubber. J Mech Phys Solids 2011;59(2):473–95.
[6] Pouca MCPV, Areias P, Göktepe S, Ashton-Miller JA, Jorge RMN, Parente MPL. Modeling permanent deformation during low-cycle fatigue: Application to the pelvic floor muscles during labor. J Mech Phys Solids 2022;164:104908.
[7] Movahedi-Rad AV, Keller T, Vassilopoulos AP. Fatigue damage in angle-ply GFRP laminates under tension-tension fatigue. Int J Fatigue 2018;109:60–9.
[8] Rana D, Sauvant V, Halary JL. Molecular analysis of yielding in pure and antiplasticized epoxy-amine thermosets. J Mater Sci 2002;37:5267–74.
[9] Plaseied A, Fatemi A. Deformation response and constitutive modeling of vinyl ester polymer including strain rate and temperature effects. J Mater Sci 2008;43:1191–9.
[10] Yan L, Chouw N, Jayaraman K. Effect of UV and water spraying on the mechanical properties of flax fabric reinforced polymer composites used for civil engineering applications. Mater Des 2015;71:17–25.
[11] Malpot A, Touchard F, Bergamo S. Influence of moisture on the fatigue behaviour of a woven thermoplastic composite used for automotive application. Mater Des 2016;98:12–9.
[12] Savvilotidou M, Keller T, Vassilopoulos AP. Fatigue performance of a cold-curing structural epoxy adhesive subjected to moist environments. Int J Fatigue 2017;103:405–14.
[13] Wang X, Zhao X, Wu Z. Fatigue degradation and life prediction of basalt fiber-reinforced polymer composites after saltwater corrosion. Mater Des 2019;163:107529.
[14] Miyano Y, Nakada M, McMurray MK, Muki R. Prediction of flexural fatigue strength of CRFP composites under arbitrary frequency, stress ratio and temperature. J Compos Mater 1997;31(6):619–38.
[15] Bauwens-Crowet C. The compression yield behaviour of polymethyl methacrylate over a wide range of temperatures and strain-rates. J Mater Sci 1973;8(7):968–79.
[16] Tang H, Dai H-L, Wu H. An effect of hygrothermal effects on high velocity impact event for polymer matrix composites. Appl Math Model 2021;91:653–69.
[17] Walley SM, Field JE, Pope PH, Safford NA. A study of the rapid deformation behaviour of a range of polymers. Philos Trans R Soc Lond Ser A Math Phys Sci 1989;328(1597):1–33.
[18] Rietsch F, Bouette B. The compression yield behaviour of polycarbonate over a wide range of strain rates and temperatures. Eur Polym J 1990;26(10):1071–5.
[19] Blumenthal WR, Cady CM, Lopez MF, Gray GT, Idar DJ. Influence of temperature and strain rate on the compressive behavior of PMMA and polycarbonate polymers. In: AIP conference proceedings. American Institute of Physics; 2002, p. 665–8.
[20] Williams ML, Landel RF, Ferry JD. The temperature dependence of relaxation mechanisms in amorphous polymers and other glass-forming liquids. J Am Chem Soc 1955;77(14):3701–7.
[21] Chou SC, Robertson KD, Rainey JH. The effect of strain rate and heat developed during deformation on the stress-strain curve of plastics. Exp Mech 1973;13(10):422–32.
[22] Eyring H. Viscosity, plasticity, and diffusion as examples of absolute reaction rates. J Chem Phys 1936;4(4):283–91.
[23] Ree T, Eyring H. Rheology, Vol. III. New York: Academic; 1958.
[24] Bauwens-Crowet C, Bauwens JC, Homes G. Tensile yield-stress behavior of glassy polymers. J Polym Sci A-2: Polym Phys 1969;7(4):735–42.
[25] Bueche F. Tensile strength of plastics above the glass temperature. J Appl Phys 1955;26(9):1133–40.
[26] Smith Thor L. Viscoelastic behavior of polyisobutylene under constant rates of elongation. J Polym Sci 1956;20(94):89–100.
[27] Chen Y, Zhao Z, Guo Z, Li Y. Micromechanical model of linear viscoelastic particle-reinforced composites with interphase. Appl Math Model 2021;97:308–21.
[28] Movahedi-Rad AV, Keller Thomas. A novel methodology of predicting temperature and rate effects on tensile properties of viscoelastic materials. Int J Non-Linear Mech 2024;159:104613.
[29] Spathis G, Kontou E. Creep failure time prediction of polymers and polymer composites. Compos Sci Technol 2012;72(9):959–64.
[30] Eftekhari M, Fatemi A. On the strengthening effect of increasing cycling frequency on fatigue behavior of some polymers and their composites: Experiments and modeling. Int J Fatigue 2016;87:153–66.

[31] Guster Ch, Pinter G, Mösenbacher A, Eichlseder W. Evaluation of a simulation process for fatigue life calculation of short fibre reinforced plastic components. Procedia Eng 2011;10:2104–9.
[32] Montesano J, Fawaz Z, Behdinan K, Poon C. Fatigue damage characterization and modeling of a triaxially braided polymer matrix composite at elevated temperatures. Compos Struct 2013;101:129–37.
[33] Zhao X, Wang X, Wu Z, Keller T, Vassilopoulos AP. Temperature effect on fatigue behavior of basalt fiber-reinforced polymer composites. Polym Compos 2019;40(6):2273–83.
[34] Li C, Xian G, Li H. Effect of postcuring immersed in water under hydraulic pressure on fatigue performance of large-diameter pultruded carbon/glass hybrid rod. Fatigue Fract Eng Mater Struct 2019;42(5):1148–60.
[35] Li C, Yin X, Liu Y, Guo R, Xian G. Long-term service evaluation of a pultruded carbon/glass hybrid rod exposed to elevated temperature, hydraulic pressure and fatigue load coupling. Int J Fatigue 2020;134:105480.
[36] Wan YZ, Wang YL, Huang Y, Luo HL, He F, Chen GC. Moisture absorption in a three-dimensional braided carbon/Kevlar/epoxy hybrid composite for orthopaedic usage and its influence on mechanical performance. Composites A 2006;37(9):1480–4.
[37] Sarfaraz R, Vassilopoulos AP, Keller T. Experimental investigation and modeling of mean load effect on fatigue behavior of adhesively-bonded pultruded GFRP joints. Int J Fatigue 2012;44:245–52.
[38] Petermann J, Schulte K. The effects of creep and fatigue stress ratio on the long-term behaviour of angle-ply CFRP. Compos Struct 2002;57(1–4):205–10.
[39] Vieille B, Albouy W, Taleb L. About the creep-fatigue interaction on the fatigue behaviour of off-axis woven-ply thermoplastic laminates at temperatures higher than Tg. Composites B 2014;58:478–86.
[40] Sayyidmousavi A, Bougherara H, Fawaz Z. The role of viscoelasticity on the fatigue of angle-ply polymer matrix composites at high and room temperatures-a micromechanical approach. Appl Compos Mater 2015;22:307–21.
[41] Movahedi-Rad AV, Keller T, Vassilopoulos AP. Stress ratio effect on tension-tension fatigue behavior of angle-ply GFRP laminates. Int J Fatigue 2019;126:103–11.
[42] Movahedi-Rad AV, Keller T, Vassilopoulos AP. Interrupted tension-tension fatigue behavior of angle-ply GFRP composite laminates. Int J Fatigue 2018;113:377–88.
[43] Movahedi-Rad AV, Keller T, Vassilopoulos AP. Creep effects on tension-tension fatigue behavior of angle-ply GFRP composite laminates. Int J Fatigue 2019;123:144–56.
[44] Guedes RM. Durability of polymer matrix composites: Viscoelastic effect on static and fatigue loading. Compos Sci Technol 2007;67(11–12):2574–83.
[45] Vassilopoulos AP, Manshadi BD, Keller T. Influence of the constant life diagram formulation on the fatigue life prediction of composite materials. Int J Fatigue 2010;32(4):659–69.
[46] Movahedi-Rad AV, Eslami G, Keller T. A novel fatigue life prediction methodology based on energy dissipation in viscoelastic materials. Int J Fatigue 2021;152:106457.
[47] Schijve J. Fatigue of structures and materials. Springer; 2009.
[48] Samborsky D, Mandell JF, Miller DA. Creep/fatigue response of resin infused biaxial glass fabric laminates in reversed loading. In: 32nd ASME wind energy symposium. 2014, p. 0172.
[49] Benaarbia A, Chrysochoos A, Robert G. Thermomechanical behavior of PA6. 6 composites subjected to low cycle fatigue. Composites B 2015;76:52–64.
[50] Movahedi-Rad AV, Keller T, Vassilopoulos AP. Modeling of fatigue behavior based on interaction between time-and cyclic-dependent mechanical properties. Composites A 2019;124:105469.
[51] Naderi M, Kahirdeh A, Khonsari MM. Dissipated thermal energy and damage evolution of Glass/Epoxy using infrared thermography and acoustic emission. Composites B 2012;43(3):1613–20.
[52] Chandra R, Singh SP, Gupta K1. Damping studies in fiber-reinforced composites–a review. Compos Struct 1999;46(1):41–51.
[53] Sun CT, Chan WS. Frequency effect on the fatigue life of a laminated composite. In: Composite materials: testing and design (fifth conference). ASTM International; 1979.
[54] Barron V, Buggy M, McKenna NH. Frequency effects on the fatigue behaviour on carbon fibre reinforced polymer laminates. J Mater Sci 2001;36:1755–61.
[55] Kliman V, Bílỳ M. Hysteresis energy of cyclic loading. Mater Sci Eng 1984;68(1):11–8.
[56] Hahn HT, Kim R Yo. Fatigue behavior of composite laminate. J Compos Mater 1976;10(2):156–80.
[57] Findley WN, Davis FA. Creep and relaxation of nonlinear viscoelastic materials. Courier Corporation; 2013.
[58] Internasional A. ASTM D638-14 standard test methods for tensile properties of plastic. America Society for Testing and Material; 2014.
[59] Mulliken AD, Boyce MC. Mechanics of the rate-dependent elastic–plastic deformation of glassy polymers from low to high strain rates. Int J Solids Struct 2006;43(5):1331–56.
[60] Van Breemen LCA, Engels TAP, Klompen ETJ, Senden DJA, Govaert LE. Rate-and temperature-dependent strain softening in solid polymers. J Polym Sci B: Polym Phys 2012;50(24):1757–71.
[61] Reifsnider K, Talug A. Analysis of fatigue damage in composite laminates. Int J Fatigue 1980;2(1):3–11.
[62] Harris B. Fatigue in composites: science and technology of the fatigue response of fibre-reinforced plastics. Woodhead Publishing; 2003.